Enantioselective optical forces and size-dependent sorting of single chiral particles using vortex beams

R. Ali [1,*] F. A. Pinheiro [2] R. S. Dutra [3] T. P. Mayer Alegre [1] and G. S. Wiederhecker[1,†]

[1]*Applied Physics Department, Gleb Wataghin Physics Institute, University of Campinas, Campinas, São Paulo 13083-859, Brazil*
[2]*Instituto de Física, Universidade Federal do Rio de Janeiro, Caixa Postal 68528, Rio de Janeiro, Rio de Janeiro 21941-972, Brazil*
[3]*LISComp-IFRJ, Instituto Federal de Educação, Ciência e Tecnologia, Rua Sebastião de Lacerda,*
Paracambi, Rio de Janeiro 26600-000, Brazil

We put forward an approach to manipulate and enantioselect chiral microspheres using vortex beams that encode topological charges. Vortex beams with different topological charges transfer angular momentum to chiral particles with opposite handedness in a different way. This process also depends on the incident polarization, in a rich interplay that ultimately leads to enantioselective optical forces acting on single chiral particles with selected, arbitrary sizes. Besides this scheme also depends on the order of the topological charge, which can also be controlled experimentally. The resulting enantioselective optical forces are up to two orders of magnitude larger than the existing chiral resolution methods based on optical forces, further demonstrating the unique functionalities and applicability of the method.

I. INTRODUCTION

The concept of chirality, introduced by Lord Kelvin to designate any geometrical object or ensemble of points that lack mirror symmetry, pervades the natural world [1]. Such nonsuperimposable mirror images, so-called left- and right-handed chiral enantiomers [2–4], interact with electromagnetic fields in a different way [5,6]. Electromagnetic manifestations of chirality have several technological and scientific applications and hence distinguishing chiral materials with opposite handedness is an important, sought-after goal [1]. Different enantioselective strategies have been proposed and constitute the focus of an extensive and multidisciplinary research field. One of the most traditional strategies for enantioselection is to exploit the optical response of chiral materials, such as the optical rotatory power and circular dichroism [7,8].

Recent advances in nanophotonics have enabled the design of single nanoparticles with significantly enhanced optical chiral response, when compared to natural chiral materials [8–12]. However, traditional probes of chirality are inadequate for studying single chiral nanoparticles with unknown properties [13,14]. To overcome this limitation, alternative enantioselective optical methods have been proposed, such as optical tweezing [15–24] and pulling forces [25–34], which enable the enantioselection of nanoparticles by using optical forces.

Previous studies have primarily utilized circularly polarized (CP) Gaussian beams to exert chirality-dependent optical trapping forces and pulling/pushing forces. However, these methods often require high laser power or numerical apertures to exert oppositely directed forces on particles of specific geometric and optical parameters. In this regard, flexibility can be achieved by considering the beam that shows reconfigurable interaction with the chirality of the sphere. For instance, CP vortex beam carries spin angular momentum (SAM) with bounded values of $\pm\hbar$ per photon ($\hbar$ is Planck's constant divided by 2π), which is weaker compared to the orbital angular momentum (OAM), defined by $\ell\hbar$ per photon [35,36], where ℓ is the topological charge [37]. Such reconfigurable light-matter iterations can provide fertile ground for discussing the tunable optical forces on the sphere. Various strategies have been employed to generate a helical wavefront that carries both SAM and OAM simultaneously [36,38–41]. For example, Laguerre-Gaussian beams have been utilized to create stronger trapping potentials by leveraging their helical wavefront, which carries a large OAM [37,42–47]. This characteristic proves beneficial for trapping low-refractive-index small particles [48]. Structured vortex beams have been explored to achieve optical trapping [49] and to generate enantioselective optical gradient forces [50,51]. However, the latter scheme only applies to Rayleigh-sized chiral particles so far [51].

In this work, we investigate the interplay between the chirality parameter of microparticles and the OAM of a vortex beam to achieve optical pulling and pushing forces on single chiral spheres. Using this scheme we demonstrate the capability for enantioselection of arbitrarily sized chiral particles. The proposed scheme using vortex beams allows for stronger enantioselective optical pushing forces when compared to the ones based on focused Gaussian beams [25]. Besides the method enables efficient low-power optical traps that can be tuned by changing the angular momentum of the incident beam. Furthermore, we also show the vast applicability of

*Contact author: rali.physicist@gmail.com
†Contact author: gsw@unicamp.br

vortex beams for the optical sorting of single chiral particles with selected and arbitrary size ranges.

The proposed enantioselective scheme relies on the fact that the OAM ℓ index can assume any integer values ranging from $\{+\ell, -\ell\}$ associated with positive (left-handed helical wave front) and negative optical vortices (right-handed helical wave front), respectively [52]. Indeed, we show that the optical vortices with tunable OAM modes $(+\ell, -\ell)$ play a key role in the optical pulling force to probe the chiroptical response. Physically, vortex beams with different OAM index transfer angular momentum to chiral spheres with opposite handedness in a different way, also depending on the incident beam polarization, in a rich interplay that ultimately leads to an enantioselective optical force. Since the order of integer value of the OAM modes ℓ can be experimentally controlled [53–59], the proposed enantioselective scheme provides an alternative mechanism for characterizing the chiral optical response of isolated particles using optical pulling forces.

II. THEORETICAL FRAMEWORK

Laguerre-Gaussian beams have a well-defined forward momentum $\hbar k_z$, where k_z is the wave number along the z axis, and helical phase $e^{(i\ell\phi)}$, where ℓ is known as topological charge and ϕ is the azimuthal angle [52,56–60].

To describe the spatial profile of Laguerre-Gaussian beams, a rigorous theoretical framework is adopted. We consider a circularly polarized vortex beam of helicity σ, topological charge ℓ, and vacuum wave number $k_0 = 2\pi/\lambda_0$, wavelength in vacuum λ_0, propagating along the $+z$ direction

$$\mathbf{E}_{in} = E_0 e^{i(k_0 z - \omega t)} e^{i\ell\varphi}(\hat{\mathbf{x}} + i\sigma\hat{\mathbf{y}}), \qquad (1)$$

where E_0 is the incident electric field amplitude. We consider a collimated incident beam at the objective entrance with a well-defined polarization state in this derivation. This description is obtained in the paraxial limit where $k_z \approx k_0$. After impinging on an objective lens of focal length f, with a narrow annular aperture on its entrance [37,61], the resulting beam is a nonparaxial vortex beam with an aperture angle θ. The nonparaxial beam in the focal region is described by the formalism of the Richards and Wolf diffraction integrals [62–64], which in physical terms means superimposing in the reciprocal space the different Fourier components belonging to the surface of a cone with aperture angle θ. The target chiral particles are assumed to be located at the focal plane inside an aqueous solution, as illustrated in Fig. 1.

We consider an objective of focal length f, with a narrow annular aperture on its entrance [37,61]. This setup creates a nonparaxial vortex beam with aperture angle θ focused onto the sample chamber containing an aqueous solution and chiral microsphere. The mathematical description of this conical-shaped beam in the focal plane is described in terms of the Richards and Wolf model; see details in Appendix A.

The interaction between the resulting field distribution [see Eq. (A2)] and a Mie chiral microsphere: of radius a, electric permittivity ε, chirality κ, and refractive index $n_p = \sqrt{\varepsilon} + \sigma\kappa$ can be described using the Debye potential formalism [65,66].

Due to the spherical symmetry of the scattering center, the incident nonparaxial conic beam and scattered electromagnetic field distribution have been expanded in terms of
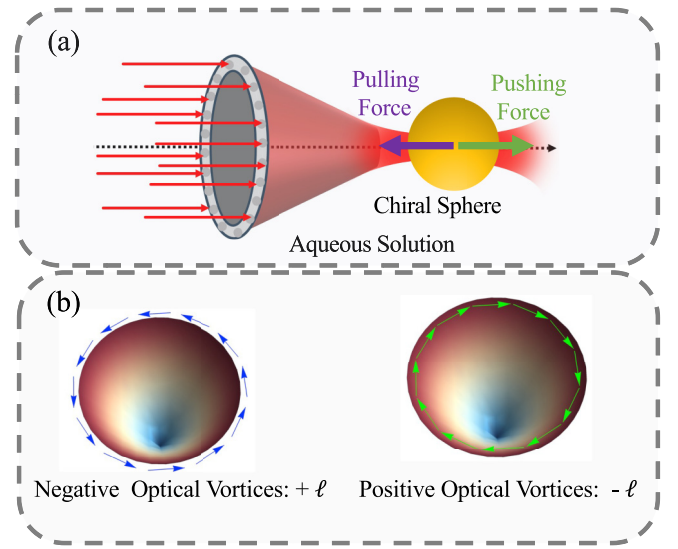

FIG. 1. Schematic illustration of incident conic beam: (a) circularly polarized plane waves are entering the objective and forming a hollow conical vortex beam carrying topological charge appearing due to its helical wavefront. The resulting optical pulling (purple arrow) and pushing force (green arrow) acting on the chiral sphere to the incident beam are also shown. (b) Top view of the hollow conic vortex beam showing (b) the left-handed helical wavefront with topological order $+\ell$ and right-handed helical wavefront with topological order $-\ell$.

spherical waves using the Debye potential formalism [65,66]. The electric (E) and magnetic (M) scattered Debye potentials, describing outgoing waves, using Hankel functions $h_j^{(1)}(kr)$ and spherical harmonics $Y_{j,m}(\Theta, \Phi)$, are given by

$$\Pi_s^E = -\sigma \frac{f n_h E_0}{\lambda_0 k} \sum_{j,m} A_j \gamma_{jm} Y_{j,m}(\Theta, \Phi) h_j^{(1)}(kr) \qquad (2)$$

and

$$\Pi_s^M = i \frac{f n_h H_0}{\lambda_0 k} \sum_{j,m} B_j \gamma_{jm} Y_{j,m}(\Theta, \Phi) h_j^{(1)}(kr), \qquad (3)$$

with incident amplitudes γ_{jm}

$$\gamma_{jm} = \sqrt{\frac{4\pi(2j+1)}{j(j+1)}} 2\pi(i)^j(-i)^{(m-\sigma-\ell)} e^{-i(m-\sigma-\ell)\phi_s}$$

$$\times d_{m,\sigma+\ell}^j(\theta) J_{m-\sigma-\ell}(k\rho_s \sin\theta) e^{ik z_s \cos\theta}, \qquad (4)$$

coming from the focused electric field, Eq. (A2), after expanding it in terms of spherical waves, with standard cylindrical coordinates (ρ_s, ϕ_s, z_s) representing the microsphere position in relation to the focal point. The sums over multipole expansions are explicitly given by $\sum_{jm}(\ldots) \equiv \sum_{j=1}^{\infty} \sum_{m=-j}^{j}(\ldots)$. The Wigner rotation matrices $d_{m,m'}^j$ [67] define the rotation of each plane wave that composes the conic beam with aperture angle θ. The spherical coordinates (r, Θ, Φ) describe a point of the outgoing spherical wave fronts.

The coefficients A_j and B_j, appearing in Eqs. (2) and (3), are effective Mie coefficients for the chiral sphere, which are detailed in Appendix B.

For future reference, one can define the scattered electric $\mathbf{E}_s$ and scattered magnetic $\mathbf{H}_s$ fields by the chiral sphere using Eqs. (2) and (3) under the action of the appropriate vector operators [66]. Once the total electric $\mathbf{E} = \mathbf{E}_{in} + \mathbf{E}_s$ and total magnetic $\mathbf{H} = \mathbf{H}_{in} + \mathbf{H}_s$ fields are found, we are able to obtain the optical force imparted on the chiral sphere by integrating the Maxwell stress tensor over a spherical Gaussian surface at infinity:

$$\mathbf{F} = \lim_{r \to \infty} \left[-\frac{r}{2} \int \mathbf{r}(\epsilon_h \epsilon_0 E^2 + \mu_0 H^2) d\Omega \right], \quad (5)$$

where ϵ_0 and μ_0 are the vacuum permittivity and permeability, respectively. The total optical force acting on the sphere has two distinct force components, namely scattering force F_{sz} and extinction force F_{ez} being associated with the scattered field $\mathbf{E}_s \cdot \mathbf{E}_s^*$ and the interference between the incident and scattered field $\mathbf{E}_{\rm inc} \cdot \mathbf{E}_s^*$, respectively. Since the incident plane waves have the same amplitude and polarization with well-defined momentum in the forward direction, the net optical force will point along the z axis by symmetry. Calculating the flux of the Maxwell stress tensor, taking the total electromagnetic field outside the microsphere, over a large Gaussian surface, extending to infinity, we obtain the scattered axial (taking $\rho_s = 0$) optical force so that only the far field distribution contributes [25,68]

$$
\begin{aligned}
F_{sz} = {} & -\frac{16\pi^3 E_0^2}{k^2} \mathrm{Re} \sum_j \frac{\sqrt{j(j+2)(j+\sigma+\ell+1)(j-\sigma-\ell+1)}}{j+1} \left[(A_j A_{j+1}^* + B_j B_{j+1}^*) d_{\sigma+\ell,\sigma+\ell}^j(\theta) d_{\sigma+\ell,\sigma+\ell}^{j+1}(\theta) \right] \\
& -\frac{16\pi^3 E_0^2}{k^2} \sigma(\sigma+\ell) \mathrm{Re} \sum_j \frac{(2j+1)}{j(j+1)} A_j B_j^* \left| d_{\sigma+\ell,\sigma+\ell}^j(\theta) \right|^2
\end{aligned}
\tag{6}
$$

and the extinction component

$$F_{ez} = \frac{8\pi^3 E_0^2}{k^2} \mathrm{Re} \sum_j (2j+1)(A_j + B_j) \left| d_{\sigma+\ell,\sigma+\ell}^j(\theta) \right|^2 \cos\theta. \quad (7)$$

The net force on the chiral sphere along z axes is given as

$$F_z = F_{ez} + F_{sz}. \quad (8)$$

III. RESULTS AND DISCUSSION

Based on our analytically derived expression for optical force presented in Eq. (8), we analyze the optical force dependence on the size of the sphere a, chirality parameter κ, the topological charge of the vortex beam ℓ, and on parameters that can be externally controlled such as the incident angle θ and polarization of the beam σ. In what follows, we consider a chiral sphere of refractive index $n_p = \sqrt{2.5} + \kappa$, immersed in water of refractive index $n_h = 1.332$ and chirality parameter κ, illuminated by the proposed vortex beam, as shown in Fig. 1, of vacuum wavelength $\lambda_0 = 1064$ nm. In the numerical analysis, we normalize the optical force to $F_0 = 2\pi n_h I_0/(k_2 c)$, where $I_0 = \sqrt{\epsilon_h \epsilon 0/\mu_0} E_0^2/2$ is the intensity each incident plane waves. The incident angle θ is related with objective numerical aperture NA through relation $\theta = \sin^{-1}(NA/n_w)$. For instance, a typical aperture angle of $\theta = 70°$ corresponds to a numerical aperture $NA \approx 1.25$. In the numerical calculations, we consider a beam with a large waist, corresponding to the plane wave approximation used to describe the incident beam on the objective.

In Fig. 2, we calculate the optical force acting on the chiral sphere of radius $a = 500$ nm as a function of cone angle for different integer values of the topological charge ($\ell = 0, \pm1$) and chirality parameter, where we take $\sigma = +1 \, (-1)$ for the left (right) column of Fig. 2. The results show that optical force is always positive at an angle $\theta = 0°$, as illustrated in Fig. 2, for all topological integer values. This is due to the fact that a plane wave in the paraxial domain can never exert negative optical force on a passive sphere as required by the conservation of the total optical momentum. As we increase the incident angle, Fig. 2(a) shows that the left-handed chiral spheres of chirality parameter $\kappa = 0.3$ (with the same chiral handedness as of the incident beam, i.e., $\sigma = 1$) are subjected to an optical pulling force at an angle $\theta \geqslant 75°$. On the other hand, the right-handed chiral spheres of chirality parameter $\kappa = -0.3$ (opposite-handed particles with respect to the incident beam, i.e., $\sigma = 1$) experience optical pushing force for all
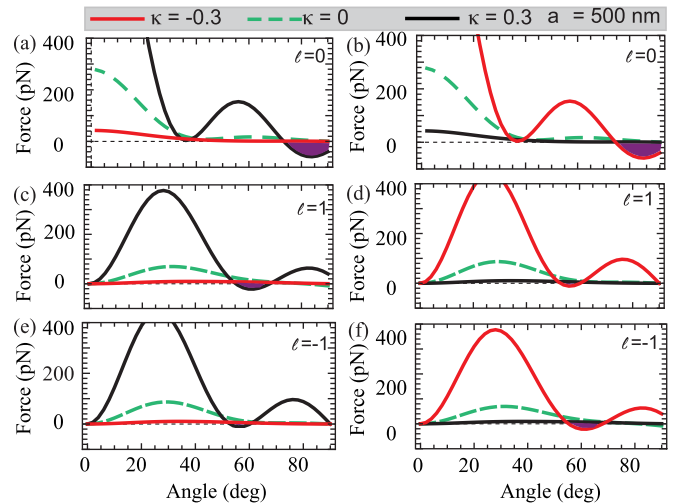

FIG. 2. Optical force acting on the chiral sphere of radius 500 nm chirality parameter: $\kappa = -0.3$ (red), $\kappa = 0$ (dashed), and $\kappa = 0.3$ (black) as a function of cone angle θ. The forces in the left(right) column are calculated by using $\sigma = +1(-1)$. The optical forces are pseudosymmetric and can be reverted to the opposite chiral enantiomer by changing the incident polarization and sign of the topological charge ℓ simultaneously as illustrated by Figs. 2(c)–2(f) and Figs. 2(d) and 2(e).

angles. In order to exert the pulling force on the right-handed chiral sphere one may revert the polarization of the incident beam as illustrated by Fig. 2(c), where the right-handed chiral spheres are attracted toward the source and left-handed particles are pushed away. Thus forces can be reversed on the chiral enantiomers by changing the polarization of the beam for $\ell = 0$ as required by symmetry. In addition, achiral particles, i.e., $\kappa = 0$, are always pushed away for both polarization due to weak interaction between the field and chiral sphere.

On the contrary, for $\ell = \pm 1$ optical force strongly depends on topological charge as well as the polarization of the beam and chirality parameter as illustrated in Figs. 2(c)–2(f). In this case, the optical pulling force appears on a sphere with matched handedness. For instance, in Figs. 2(c) and 2(f) pulling forces appear around $\theta = 56°$ in the situation where the handedness of the chiral sphere matches the handedness of the incident polarization. Similar trends are seen in Figs. 2(d) and 2(e) around angle $\theta = 53°$. For these particular configurations, the optical force can be reverted by changing the incident polarization and the sign of ℓ simultaneously as required by symmetry, i.e., $F(\sigma, \kappa, \ell) = F(-\sigma, -\kappa, -\ell)$, and shown in Figs. 2(c)–2(f).

Altogether, Fig. 2 demonstrates the nature of the optical force acting on the chiral sphere is due to the structured incident beam and is related to the spin-orbit interaction of light. Indeed, when the vortex and helicity have the same sign the net force can be pulling, whereas when they have opposite signs the net optical force is always pushing. In our approach, the additional, experimentally controllable degree of freedom related to the topological charge and its interplay with the polarization state of the incident beam provides an optimal way of controlling the direction of optical forces, allowing for the enantioselective transport of chiral spheres. It is also important to mention that a linearly polarized vortex beam can distinctively interact with achiral/chiral spheres but cannot distinguish the handedness of the chiral spheres [25].

The key finding of this work is the dependence of the enantioselective force on the topological charge ℓ and the polarization of the incident beam which singles out the proposed approach in comparison to the existing chiral resolution methods based on optical forces. Physically, vortex beams with different ℓ distinctively transfer angular momentum to chiral spheres which also depend on the incident polarization. This interplay of the selective interactions of ℓ, κ, and σ ultimately leads to an externally tunable enantioselective optical force. To further explore the implications of this finding, in Fig. 3 we calculate the optical force as a function of the sphere radius for fixed polarization $\sigma = 1$ and incident angle $\theta = 70°$ for different integer values of the topological charge ℓ and chiral parameter. Figure 3 unveils the role of topological charge on the optical pulling force. Indeed an incident beam with different values of ℓ is able to pull chiral spheres of same handedness with a wide range of radii. For instance, a sphere of radius 200 nm with chiral parameter $\kappa = +0.3$ ($\kappa = -0.3$) experiences optical pulling (pushing) force due to a left circularly polarized beam with topological charge $\ell = 0$ as shown in 3(a). In comparison to other enantioselective approaches based on optical forces, pulling force on such a small chiral sphere cannot be achieved [25,69].
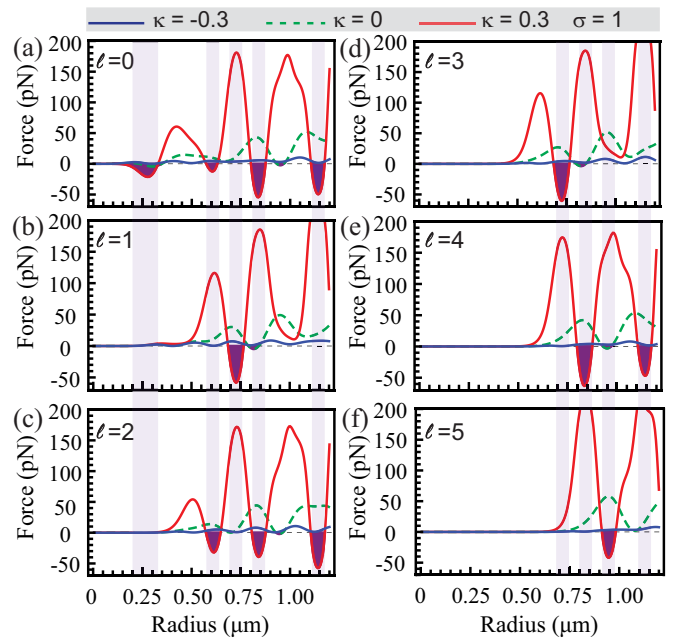

FIG. 3. Optical force as a function of sphere radius with chirality parameter: $\kappa = -0.3$ (blue), $\kappa = 0$ (dashed), and $\kappa = 0.3$ (red) at fixed indent angle $\theta = 70°$. Here we take a left circular polarized beam and different topological charge ℓ as indicated in each figure. The rest of the parameters are the same as we have taken in Fig. 2.

Figure 3 also unveils another aspect of this enantioselective scheme: the possibility of chiral resolution for specific particle size ranges. Indeed, beams with different values of ℓ can be used to selectively pull chiral spheres with a given size and handedness. For instance, Fig. 3 shows that a left-handed chiral sphere of chirality parameter $\kappa = 0.3$ and radii of approximately 600 nm, 700 nm, 850 nm, and 950 nm can only be pulled by a left circularly polarized light with topological charge $\ell = 0, 2$ [as shown in Figs. 3(a) and 3(c)], $\ell = 1, 3$ [as shown in Figs. 3(b) and 3(d)], $\ell = 0, 2, 4$ [as shown in Figs. 3(a), 3(c) and 3(e)], and $\ell = 5$ [as shown in Fig. 3(f)], respectively. It is worth noting that, in all these cases, only left-handed spheres experience an optical pulling force due to the fact that the chiral sphere enhances the light scattering when the polarization of the incident field has the same handedness as that of the chiral sphere [34]. As a result of this strong scattering, the interference between the different scattering channels, and their relative phases, maximizes the scattered momentum in the forward direction. Thus the particle experiences a significant restoring force. Therefore, a net pulling force is achieved, which can be controlled by the incident polarization helicity and topological charge. Thus, using this scheme, one can not only perform enantioselection of the chiral sphere but also perform size selection of the chiral sphere, as shown in Table I, where the chiral selection of the desired size sphere can be carried out at will by changing the integer value of the topological charge. This result demonstrates the possibility of enantioselective sorting of chiral particles according to their size, in contrast to other chiral resolution mechanisms using vortex beams [51].

It is important to mention that the sphere immersed in water should be subjected to Brownian motion and hence,

TABLE I. Summary of the main functionalities that can be achieved with the different orders of topological charge as discussed in Fig. 4. The force is pulling on the 250 nm particle for $\ell = 0$, 750 nm can be pulled for $\ell = -1$, and sphere of radius 1000 nm sphere can be pulled for $\ell = -1$. Thus the order of the topological charge allows one to perform chiral section as well as size selection.

Radius	Pulling force	Pushing force	Enantioselection
250 nm	$\ell = 0$	$\ell = \pm 1$	Yes
750 nm	$\ell = \pm 1$	$\ell = 0$	Yes
1000 nm	$\ell = 1$	$\ell = 0, -1$	Yes

according to the fluctuation-dissipation theorem, the sphere should be subjected to the Brownian force, which can be expressed as $F_B = \sqrt{12\pi\eta a k_\beta T}$ [70]. Here, a is the sphere radius, η is fluid viscosity, k_β is Boltzmann constant, and T is room temperature (300 K). For the case of a subwavelength particle, say $a = 500$ nm, immersed in the water of viscosity $\eta = 7.9 \times 10^{-4}$ Pa s [70,71], the Brownian force acting on the sphere is $F_B \approx 6$ fN [71,72]. However, the results of Figs. 2 and 3 show that the optical forces acting on the sphere are larger than the Brownian force even for weak incident intensities $I_0 = 1$ mW/μm². Thus the optical pulling and pushing forces are stable and elongated toward and away from the laser source, respectively.

In order to further understand the dependence of the proposed enantioselective mechanism on the topological charge, in Fig. 4 the optical force is calculated as a function of sphere radius and chirality parameter κ, where we take the LCP incident beam with incident angle $\theta = 70°$. Here colored regions illustrate the parameter space where the spheres experience the optical pulling force. Figure 4 highlights two major characteristics of this enantioselective mechanism that singles it out with respect to existing ones. First, in all cases, chiral particles with a given handedness are subjected to optical pulling force while other ones experience pushing force, allowing for chiral resolution for arbitrary small chiral parameters. Second, Fig. 4 shows that the conic vortex beam can not only selectively pull and push the chiral spheres with selected sizes but also one can achieve pulling forces for particles with arbitrarily small chiral indexes by varying the topological charge. This latter finding suggests that one could achieve enantioselection of spheres made of a naturally occurring material by varying the topological charge. To put in evidence these results, let us consider different cases in Figs. 4(a), 4(c), and 4(f) indicated by blue stars: a sphere of radius $a = 250$ nm with chirality parameter $\kappa = 0.2$ is subjected to negative optical forces for $\ell = 0$ and pushing force for $\ell = |1|$. In contrast, a sphere of radius $a = 750$ nm with chirality parameter $\kappa = 0.2$, as indicated by a black cross, is subjected to positive optical force for $\ell = 0$ and negative force for $\ell = |1|$. Similarly, a sphere of radius $a = 550$ nm with chirality parameter $|\kappa| = 0.05$ is subjected to pushing force when $\ell = 0$ and to pulling force for $\ell = 1$, hampering enantioselection as shown in Figs. 4(a) and 4(c), respectively. However, for $\ell = -1$ the sphere with $\kappa = 0.05$ and $\kappa = -0.05$ are subjected to optical pulling and optical pushing forces, respectively, as shown in Fig. 4(e) and indicated by blue arrows.
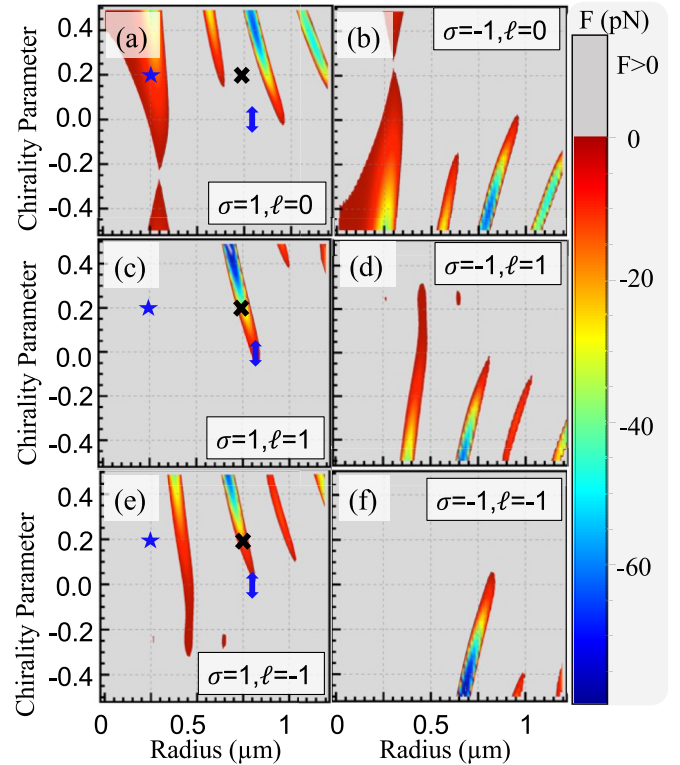

FIG. 4. Optical force as a function of the radius of the sphere and chirality parameter for fixed incident angle $\theta = 70°$. The forces in the left(right) column are calculated by using $\sigma = +1(-1)$, where the topological charge is taken as (a), (b) $\ell = 0$, (c), (d) $\ell = 1$, and (e), (f) $\ell = -1$. The other parameters are the following: refractive index of the particle and surrounding medium are $n_p = 1.58 + \kappa$ and $n_h = 1.332$, respectively.

The incident optical field is composed of multiple plane waves with well-defined propagation directions in the forward direction, e.g., along the z axis. Thus the analysis of the z components of the force is sufficient for investigating long-range manipulation. By controlling the polarization and topological charge one can selectively accelerate a chiral sphere with a given handedness due to the long-ranged pulling force towards the laser source (negative z direction), while chiral particles with opposite handedness can be accelerated towards the propagation direction (positive z axis), allowing us to perform enantioselection of chiral sphere with small chirality parameter. Indeed, in this case, particles with negative chirality parameters can be collected toward the source by using the right circularly polarized plane waves, as can be seen in Figs. 4(b), 4(d), and 4(f). In addition to chiral separation, this approach also provides an opportunity for size sorting of the chiral sphere by varying topological charges, as Fig. 4 confirms.

In order to elucidate the role of incident angle on the optical pulling force, in Fig. 5 we calculate density plots of optical force as a function of sphere radius a and the chiral parameter κ for LCP incident field impinging at different cone angles such as $\theta = 65°$ [Figs. 5(a) and 5(b)] and $\theta = 75°$ [Figs. 5(c) and 5(d)]. Figures 5(a) and 5(c) ($\ell = 0$) show that the optical pulling forces are large for large incident cone angle, e.g.,
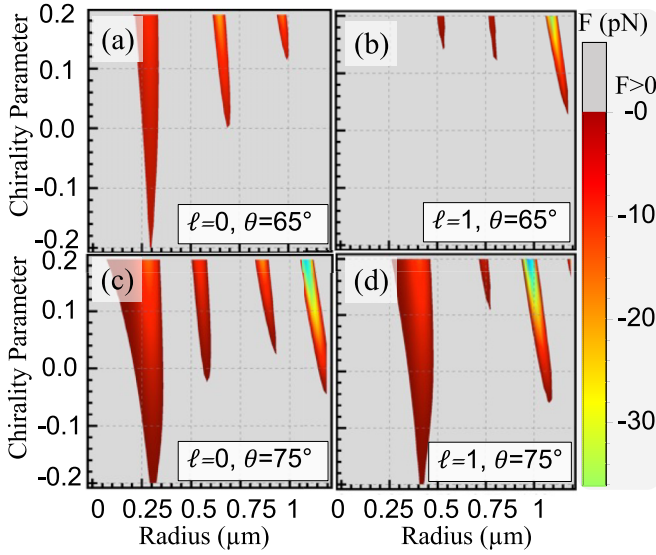
FIG. 5. Optical force as a function of the radius of the sphere and chirality parameter for fixed incident polarization $\sigma = 1$. The topological charge and cone angle are indicated in each figure, where color areas show pulling force and gray color shows pushing force.

$\theta = 75°$, where the optical pulling forces can be exerted to even the opposite-handed chiral spheres. It is important to mention that the enantioselective forces can be tuned by reducing the incident laser power so that the opposite-handed sphere can be washed out due to the Brownian motion of the particles. A similar trend is seen in Figs. 5(b) and 5(d) where $\ell = 1$. Thus it has been demonstrated that the externally controllable variable θ can allow a pathway to exert a selective optical pulling force on the one-handed chiral sphere and allow one to perform enantioselection of the selected sized chiral sphere on demand. We emphasize that optical sorting of isolated chiral particles with a small chiral response is a sought-after, challenging task that we can address here. Indeed, in Fig. 5 we show that, by tuning the cone angle, the crossover between pulling and pushing force can be tuned even for particles with very small chirality parameter.

IV. CONCLUSION

We have put forward a mechanism that allows for optical sorting and enantioselection of single chiral particles under the illumination of conic vortex beams carrying topological charges. Using the Wigner rotation matrix, we derive an explicit expression for the optical force on a chiral sphere of arbitrary size, beyond the dipolar approximation. We show that the proper combination of circularly polarized waves carrying nonzero topological charge allows one to optimize the optical enantioselective mechanism, as this leads to an increase of the magnitude of the optical forces by two orders of magnitude in comparison to previous works. Using vortex beams, the proposed enantioselective scheme also provides unprecedented control over the optical manipulation of chiral spheres of different sizes, handedness, and chiral strengths. Indeed, our findings demonstrate that the proposed scheme can not only perform enantioselection but

also the sorting of chiral particles with different sizes and chirality parameters, which solely depends on experimentally controlled parameters such as polarization and order of the topological charge.

APPENDIX A: DESCRIPTION OF THE INCIDENT BEAM

We consider a circularly polarized field entering to the objective of focal length f as described by Eq. (1) and pictorially illustrated in Fig. 1. The objective rotates the incident field to a generic direction and creates nonparaxial vortex beam with aperture angle θ that can be defined as [62,73,74]

$$\mathbf{E}(\mathbf{r}) = \frac{-i f n_m E_0}{\lambda_0} \int_0^{2\pi} d\varphi \, e^{i\mathbf{k}\cdot\mathbf{r}} \hat{\varepsilon}'(\theta, \varphi), \qquad (A1)$$

where $\hat{\varepsilon}'(\theta, \varphi) = \hat{\mathbf{x}}' \pm i\hat{\mathbf{y}}'$ defines the rotation of the plane wave contained in a cone shell, with fixed aperture angle θ, obtained by rotation with Euler angles. Integrating over azimuthal angle φ gives the electric field distribution as a function of cylindrical coordinates (z, ρ, ϕ), in relation to the focal point:

$$\mathbf{E}(\rho, \phi, z) = \frac{-i f n_m E_0}{\lambda_0} [(I_1(\rho, \phi, z) + I_2(\rho, \phi, z))\hat{\mathbf{x}} \\ + i(I_2(\rho, \phi, z) - I_1(\rho, \phi, z))\hat{\mathbf{y}} + I_0(\rho, \phi, z)\hat{\mathbf{z}}], \tag{A2}$$

where

$$I_0(\rho, \phi, z) = 2\pi(i)^{\sigma+\ell} e^{i(\sigma+\ell)\phi} \sin\theta \\ \times J_{-\sigma-\ell}(k\rho \sin\theta) e^{ikz\cos\theta}, \tag{A3}$$

$$I_1(\rho, \phi, z) = \pi(i)^{\sigma+\ell+1} e^{i(\sigma+\ell+1)\phi} (\cos\theta - \sigma) \\ \times J_{-1-\sigma-\ell}(k\rho \sin\theta) e^{ikz\cos\theta}, \tag{A4}$$

and

$$I_2(\rho, \phi, z) = \pi(i)^{\sigma+\ell-1} e^{i(\sigma+\ell-1)\phi} (\cos\theta + \sigma) \\ \times J_{1-\sigma-\ell}(k\rho \sin\theta) e^{ikz\cos\theta}. \tag{A5}$$

APPENDIX B: LIGHT SCATTERING BY A CHIRAL CHIRAL SPHERE

Consider an electromagnetic field $\mathbf{E}_{in}$ illuminating a chiral particle of radius a, immersed in a nonmagnetic dielectric host medium of refractive index n_h. By following the Bohren decomposition method [75,76], we express the electromagnetic

field in terms of the linear combinations of the vector wave functions in spherical coordinates as

$$\mathbf{E}_{in} = E_0 \sum_{\ell=1}^{\infty} i^{\ell} \frac{2\ell+1}{\ell(\ell+1)} \big(M_{o1\ell}^{(1)} - i N_{e1\ell}^{(1)} \big), \tag{B1}$$

$$\mathbf{H}_{in} = H_0 \sum_{\ell=1}^{\infty} i^{\ell} \frac{2\ell+1}{\ell(\ell+1)} \big(M_{e1\ell}^{(1)} + i N_{o1\ell}^{(1)} \big), \tag{B2}$$

where $M_{e1\ell}$, $M_{o1\ell}$, $N_{e1\ell}$, and $N_{o1\ell}$ are the vector spherical harmonics [75] with $H_0 = \frac{k}{\omega\mu} E_0$. Inside the chiral media the electric $\mathbf{E}$ and magnetic $\mathbf{H}$ fields are coupled through a phonological constant κ called chirality parameter. Therefore, the electromagnetic fields inside the chiral media can be described by the following modified constitutive relations as [75]

$$\mathbf{D} = \epsilon_0 \epsilon \mathbf{E} + i\kappa \sqrt{\epsilon_0 \mu_0}\, \mathbf{H},$$
$$\mathbf{B} = -i\kappa \sqrt{\epsilon_0 \mu_0}\, \mathbf{E} + \mu\mu_0 \mathbf{H}, \tag{B3}$$

where $\mathbf{D}$ and $\mathbf{B}$ are the electric displacement and the magnetic field, respectively. Furthermore, ϵ_0 (μ_0) is the vacuum permittivity (permeability). By using these constitutive relations in Maxwell's equations in the frequency domain, the coupling between the $\mathbf{E}$ and $\mathbf{H}$ can be removed through a linear transformation [20]. In addition, the decoupling process also suggests that the wave vector k inside the chiral media is modified which can be defined as $k_{\pm} = (\sqrt{\epsilon} \pm \kappa) k_0$, where $k_0 = 2\pi/\lambda_0$ with vacuum wavelength λ_0. Finally, one can define the scattered field by the chiral sphere in the surrounding medium as [75]

$$\mathbf{E}_s = E_0 \sum_{\ell}^{\infty} (i)^{\ell} \frac{2\ell+1}{\ell(\ell+1)} \big(i a_{\ell} N_{e1\ell}^3 - b_{\ell} M_{o1\ell}^3 + c_{\ell} M_{e1\ell}^3 - i d_{\ell} N_{o1\ell}^3 \big),$$

$$\mathbf{H}_s = H_0 \sum_{\ell}^{\infty} (i)^{\ell} \frac{2\ell+1}{\ell(\ell+1)} \big(a_{\ell} M_{e1\ell}^3 + i b_{\ell} N_{o1\ell}^3 - i c_{\ell} N_{e1\ell}^3 - d_{\ell} M_{o1\ell}^3 \big),$$
$$\tag{B4}$$

where a_{ℓ}, b_{ℓ}, c_{ℓ}, and d_{ℓ} are commonly known as Mie coefficients. Applying the boundary conditions on the microsphere surface, one can obtain [76]

$$a_{\ell} = \frac{V_{\ell}(-)A_{\ell}(+) + V_{\ell}(+)A_{\ell}(-)}{W_{\ell}(+)V_{\ell}(-) + V_{\ell}(+)W_{\ell}(-)},$$

$$b_{\ell} = \frac{W_{\ell}(+)B_{\ell}(-) + W_{\ell}(-)B_{\ell}(+)}{W_{\ell}(+)V_{\ell}(-) + V_{\ell}(+)W_{\ell}(-)},$$

$$c_{\ell} = -d_{\ell} = i\frac{W_{\ell}(-)A_{\ell}(+) - W_{\ell}(+)A_{\ell}(-)}{W_{\ell}(+)V_{\ell}(-) + V_{\ell}(+)W_{\ell}(-)}, \tag{B5}$$

with

$$W_{\ell}(\sigma) = m\psi_{\ell}(y_{\sigma})\xi_{\ell}'(x) - \xi_{\ell}(x)\psi_{\ell}'(y_{\sigma}),$$

$$V_{\ell}(\sigma) = \psi_{\ell}(y_{\sigma})\xi_{\ell}'(x) - m\xi_{\ell}(x)\psi_{\ell}'(y_{\sigma}),$$

$$A_{\ell}(\sigma) = m\psi_{\ell}(y_{\sigma})\psi_{\ell}'(x) - \psi_{\ell}(x)\psi_{\ell}'(y_{\sigma}),$$

$$B_{\ell}(\sigma) = \psi_{\ell}(y_{\sigma})\psi_{\ell}'(x) - m\psi_{\ell}(x)\psi_{\ell}'(y_{\sigma}), \tag{B6}$$

where $m = m_+ m_- / 2(m_+ + m_-)$, $m_{\pm} = \sqrt{\epsilon} \pm \kappa$, and ψ_{ℓ} and ξ_{ℓ} are the Riccati-Bessel functions that are evaluated either at the size parameter $x = \sqrt{\epsilon_h} k_0 a$ defined with respect to the wavelength in the nonmagnetic achiral host medium (relative electric permittivity ϵ_h) or at $y_{\sigma} = m_{\sigma} x / \sqrt{\epsilon_h}$.

For the sake of convenience, we can write the effective Mie coefficients [used in Eqs. (2) and (3)] in terms of standard Mie coefficients for chiral sphere a_j, b_j, c_j, and d_j and express them as [17,77]

$$A_j = a_j + i\sigma\, d_j, \tag{B7}$$

$$B_j = b_j - i\sigma\, c_j. \tag{B8}$$

[1] G. H. Wagnière, *On Chirality and the Universal Asymmetry: Reflections on Image and Mirror Image* (VHCA Wiley-VCH, Zurich, 2007).

[2] C. W. G. W. H. Brooks and K. G. Daniel, The significance of chirality in drug design and development, Curr. Top. Med. Chem. **11**, 760 (2011).

[3] J. T. Collins, C. Kuppe, D. C. Hooper, C. Sibilia, M. Centini, and V. K. Valev, Chirality and chiroptical effects in metal nanostructures: fundamentals and current trends, Adv. Opt. Mater. **5**, 1700182 (2017).

[4] L. M. Haupert and G. J. Simpson, Chirality in nonlinear optics, Annu. Rev. Phys. Chem. **60**, 345 (2009).

[5] C. Genet, Chiral light–chiral matter interactions: an optical force perspective, ACS Photon. **9**, 319 (2022).

[6] J. Yamanishi, H.-Y. Ahn, H. Yamane, S. Hashiyada, H. Ishihara, K. T. Nam, and H. Okamoto, Optical gradient force on chiral particles, Sci. Adv. **8**, eabq2604 (2022).

[7] L. D. Barron, Symmetry and chirality: Where physics shakes hands with chemistry and biology, Isr. J. Chem. **61**, 517 (2021).

[8] L. D. Barron, *Molecular Light Scattering and Optical Activity*, 2nd ed. (Cambridge University Press, Cambridge, UK, 2004).

[9] Y. Shi, T. Zhu, T. Zhang, A. Mazzulla, D. P. Tsai, W. Ding, A. Q. Liu, G. Cipparrone, J. J. Sáenz, and C.-W. Qiu, Chirality-assisted lateral momentum transfer for bidirectional enantioselective separation, Light Sci. Appl. **9**, 62 (2020).

[10] X. Wang, M. Wang, R. Lei, S. F. Zhu, Y. Zhao, and C. Chen, Chiral surface of nanoparticles determines the orientation of adsorbed transferrin and its interaction with receptors, ACS Nano **11**, 4606 (2017).

[11] M. Hwang and B. Yeom, Fabrication of chiral materials in nano- and microscale, Chem. Mater. **33**, 807 (2021).

[12] H. Zhang, S. Li, A. Qu, C. Hao, M. Sun, L. Xu, C. Xu, and H. Kuang, Engineering of chiral nanomaterials for biomimetic catalysis, Chem. Sci. **11**, 12937 (2020).

[13] D. Qu, M. Archimi, A. Camposeo, D. Pisignano, and E. Zussman, Circularly polarized laser with chiral nematic cellulose nanocrystal cavity, ACS Nano **15**, 8753 (2021).

[14] D. V. Guzatov and V. V. Klimov, The influence of chiral spherical particles on the radiation of optically active molecules, New J. Phys. **14**, 123009 (2012).

[15] D. G. Kotsifaki, V. G. Truong, and S. N. Chormaic, Fano-resonant, asymmetric, metamaterial-assisted tweezers for single nanoparticle trapping, Nano Lett. **20**, 3388 (2020).

[16] M. G. Donato, J. Hernandez, A. Mazzulla, C. Provenzano, R. Saija, R. Sayed, S. Vasi, A. Magazzù, P. Pagliusi, R. Bartolino, P. G. Gucciardi, O. M. Maragò, and G. Cipparrone, Polarization-dependent optomechanics mediated by chiral microresonators, Nat. Commun. **5**, 3656 (2014).

[17] R. Ali, F. A. Pinheiro, R. S. Dutra, F. S. S. Rosa, and P. A. Maia Neto, Enantioselective manipulation of single chiral nanoparticles using optical tweezers, Nanoscale **12**, 5031 (2020).

[18] H. Niinomi, T. Sugiyama, A.-C Cheng, M. Tagawa, T. Ujihara, H. Y. Yoshikawa, R. Kawamura, J. Nozawa, J. T. Okada, and S. Uda, Chiral optical force generated by a superchiral near-field of a plasmonic triangle trimer as origin of giant bias in chiral nucleation: A simulation study, J. Phys. Chem. C **125**, 6209 (2021).

[19] Y. Zhao, A. A. E. Saleh, and J. A. Dionne, Enantioselective optical trapping of chiral nanoparticles with plasmonic tweezers, ACS Photon. **3**, 304 (2016).

[20] R. Ali, R. S. Dutra, F. A. Pinheiro, F. S. S. Rosa, and P. A. Maia Neto, Theory of optical tweezing of dielectric microspheres in chiral host media and its applications, Sci. Rep. **10**, 16481 (2020).

[21] D. S. Bradshaw and D. L. Andrews, Chiral discrimination in optical trapping and manipulation, New J. Phys. **16**, 103021 (2014).

[22] G. Tkachenko and E. Brasselet, Helicity-dependent three-dimensional optical trapping of chiral microparticles, Nat. Commun. **5**, 4491 (2014).

[23] Y. Zhao, A. A. E. Saleh, M. A. van de Haar, B. Baum, J. A. Briggs, A. Lay, O. A. Reyes-Becerra, and J. A. Dionne, Nanoscopic control and quantification of enantioselective optical forces, Nat. Nanotechnol. **12**, 1055 (2017).

[24] M. Li, X. Chen, S. Yan, Y. Zhang, and B. Yao, Enantioselective rotation of chiral particles by azimuthally polarized beams, Adv. Photon. Res. **3**, 2200117 (2022).

[25] R. Ali, R. Dutra, F. Pinheiro, and P. M. Neto, Enantioselection and chiral sorting of single microspheres using optical pulling forces, Opt. Lett. **46**, 1640 (2021).

[26] R. P. Cameron, S. M. Barnett, and A. M. Yao, Discriminatory optical force for chiral molecules, New J. Phys. **16**, 013020 (2014).

[27] S. B. Wang and C. T. Chan, Lateral optical force on chiral particles near a surface, Nat. Commun. **5**, 3307 (2014).

[28] K. Ding, J. Ng, L. Zhou, and C. T. Chan, Realization of optical pulling forces using chirality, Phys. Rev. A **89**, 063825 (2014).

[29] R. Ali, R. Dutra, and S. Iqbal, Tailoring radiation pressure on infinite slab using pair of non-collinear plane waves, Opt. Mater. (Amsterdam) **138**, 113639 (2023).

[30] H. Chen, C. Liang, S. Liu, and Z. Lin, Chirality sorting using two-wave-interference–induced lateral optical force, Phys. Rev. A **93**, 053833 (2016).

[31] T. Zhang, M. R. C. Mahdy, Y. Liu, J. H. Teng, C. T. Lim, Z. Wang, and C.-W. Qiu, All-optical chirality-sensitive sorting via reversible lateral forces in interference fields, ACS Nano **11**, 4292 (2017).

[32] T. Cao and Y. Qiu, Lateral sorting of chiral nanoparticles using fano-enhanced chiral force in visible region, Nanoscale **10**, 566 (2018).

[33] Y. Li, C. Bruder, and C. P. Sun, Generalized Stern-Gerlach effect for chiral molecules, Phys. Rev. Lett. **99**, 130403 (2007).

[34] R. Ali, F. A. Pinheiro, R. S. Dutra, T. P. M. Alegre, and G. S. Wiederhecker, Enantioselective optical forces in gain-functionalized single core-shell chiral nanoparticles, Phys. Rev. A **108**, 043704 (2023).

[35] Y. Fang, Z. Guo, P. Ge, Y. Dou, Y. Deng, Q. Gong, and Y. Liu, Probing the orbital angular momentum of intense vortex pulses with strong-field ionization, Light Sci. Appl. **11**, 34 (2022).

[36] Y. Guo, S. Zhang, M. Pu, Q. He, J. Jin, M. Xu, Y. Zhang, P. Gao, and X. Luo, Spin-decoupled metasurface for simultaneous detection of spin and orbital angular momenta via momentum transformation, Light Sci. Appl. **10**, 63 (2021).

[37] Y. Yang, Y. Ren, M. Chen, Y. Arita, and C. Rosales-Guzmán, Optical trapping with structured light: a review, Adv. Photon. **3**, 034001 (2021).

[38] G. Biener, A. Niv, V. Kleiner, and E. Hasman, Formation of helical beams by use of Pancharatnam–Berry phase optical elements, Opt. Lett. **27**, 1875 (2002).

[39] L. Marrucci, C. Manzo, and D. Paparo, Optical spin-to-orbital angular momentum conversion in inhomogeneous anisotropic media, Phys. Rev. Lett. **96**, 163905 (2006).

[40] L. E. de Araujo and M. E. Anderson, Measuring vortex charge with a triangular aperture, Opt. Lett. **36**, 787 (2011).

[41] J. Leach, J. Courtial, K. Skeldon, S. M. Barnett, S. Franke-Arnold, and M. J. Padgett, Interferometric methods to measure orbital and spin, or the total angular momentum of a single photon, Phys. Rev. Lett. **92**, 013601 (2004).

[42] V. Garcés-Chávez, D. McGloin, M. J. Padgett, W. Dultz, H. Schmitzer, and K. Dholakia, Observation of the transfer of the local angular momentum density of a multiringed light beam to an optically trapped particle, Phys. Rev. Lett. **91**, 093602 (2003).

[43] A. T. O'Neil, I. MacVicar, L. Allen, and M. J. Padgett, Intrinsic and extrinsic nature of the orbital angular momentum of a light beam, Phys. Rev. Lett. **88**, 053601 (2002).

[44] H.-S. Chai and L.-G. Wang, Improvement of optical trapping effect by using the focused high-order Laguerre–Gaussian beams, Micron **43**, 887 (2012).

[45] P. K. Mondal, B. Deb, and S. Majumder, Angular momentum transfer in interaction of Laguerre-Gaussian beams with atoms and molecules, Phys. Rev. A **89**, 063418 (2014).

[46] Y. Zhang, M. Li, S. Yan, Y. Zhou, W. Gao, and B. Yao, Identification and separation of chiral particles by focused circularly polarized vortex beams, J. Opt. Soc. Am. A **39**, 1371 (2022).

[47] M. Li, S. Yan, Y. Zhang, X. Chen, and B. Yao, Optical separation and discrimination of chiral particles by vector beams with orbital angular momentum, Nanoscale Adv. **3**, 6897 (2021).

[48] K. T. Gahagan and G. A. Swartzlander, Simultaneous trapping of low-index and high-index microparticles observed with an optical-vortex trap, J. Opt. Soc. Am. B **16**, 533 (1999).

[49] Z. Wu, J. Zhao, J. Dou, J. Liu, Q. Jing, B. Li, and Y. Hu, Optical trapping of multiple particles based on a rotationally-symmetric power-exponent-phase vortex beam, Opt. Express **30**, 42892 (2022).

[50] D. Green and K. A. Forbes, Optical chirality of vortex beams at the nanoscale, Nanoscale **15**, 540 (2023).

[51] K. A. Forbes and D. Green, Enantioselective optical gradient forces using 3D structured vortex light, Opt. Commun. **515**, 128197 (2022).

[52] Y. Shen, X. Wang, Z. Xie, C. Min, X. Fu, Q. Liu, M. Gong, and X. Yuan, Optical vortices 30 years on: OAM manipulation from topological charge to multiple singularities, Light Sci. Appl. **8**, 90 (2019).

[53] M. Beijersbergen, L. Allen, H. van der Veen, and J. Woerdman, Astigmatic laser mode converters and transfer of orbital angular momentum, Opt. Commun. **96**, 123 (1993).

[54] X. Cai, J. Wang, M. J. Strain, B. Johnson-Morris, J. Zhu, M. Sorel, J. L. O'Brien, M. G. Thompson, and S. Yu, Integrated compact optical vortex beam emitters, Science **338**, 363 (2012).

[55] J. Wang, J.-Y. Yang, I. M. Fazal, N. Ahmed, Y. Yan, H. Huang, Y. Ren, Y. Yue, S. Dolinar, M. Tur, and A. E. Willner, Terabit free-space data transmission employing orbital angular momentum multiplexing, Nat. Photon. **6**, 488 (2012).

[56] Z. Zhao, J. Wang, S. Li, and A. E. Willner, Metamaterials-based broadband generation of orbital angular momentum carrying vector beams, Opt. Lett. **38**, 932 (2013).

[57] E. Karimi, S. A. Schulz, I. De Leon, H. Qassim, J. Upham, and R. W. Boyd, Generating optical orbital angular momentum at visible wavelengths using a plasmonic metasurface, Light Sci. Appl. **3**, e167 (2014).

[58] M. I. Shalaev, J. Sun, A. Tsukernik, A. Pandey, K. Nikolskiy, and N. M. Litchinitser, High-efficiency all-dielectric metasurfaces for ultracompact beam manipulation in transmission mode, Nano Lett. **15**, 6261 (2015).

[59] K. E. Chong, I. Staude, A. James, J. Dominguez, S. Liu, S. Campione, G. S. Subramania, T. S. Luk, M. Decker, D. N. Neshev, I. Brener, and Y. S. Kivshar, Polarization-independent silicon metadevices for efficient optical wavefront control, Nano Lett. **15**, 5369 (2015).

[60] T. Qu, Z.-S. Wu, Q.-C. Shang, and Z.-J. Li, Light scattering of a Laguerre–Gaussian vortex beam by a chiral sphere, J. Opt. Soc. Am. A **33**, 475 (2016).

[61] D. McGloin and K. Dholakia, Bessel beams: Diffraction in a new light, Contemp. Phys. **46**, 15 (2005).

[62] E. Wolf, Electromagnetic diffraction in optical systems-I. An integral representation of the image field, Proc. R. Soc. London A **253**, 349 (1959).

[63] P. Varga and P. Török, The Gaussian wave solution of Maxwell's equations and the validity of scalar wave approximation, Opt. Commun. **152**, 108 (1998).

[64] L. Novotny, R. D. Grober, and K. Karrai, Reflected image of a strongly focused spot, Opt. Lett. **26**, 789 (2001).

[65] C. Bouwkamp and H. Casimir, On multipole expansions in the theory of electromagnetic radiation, Physica **20**, 539 (1954).

[66] A. Mazolli, P. A. M. Netoo, and H. Nussenzveig, Theory of trapping forces in optical tweezers, Proc. R. Soc. London A **459**, 3021 (2003).

[67] A. R. Edmonds, *Angular Momentum in Quantum Mechanics* (Princeton University Press, Princeton, NJ, 2016).

[68] R. Ali, F. A. Pinheiro, R. S. Dutra, and P. A. M. Neto, Tailoring optical pulling forces with composite microspheres, Phys. Rev. A **102**, 023514 (2020).

[69] H. Zheng, X. Li, H. Chen, and Z. Lin, Selective transport of chiral particles by optical pulling forces, Opt. Express **29**, 42684 (2021).

[70] K. Okamoto and S. Kawata, Radiation force exerted on sub-wavelength particles near a nanoaperture, Phys. Rev. Lett. **83**, 4534 (1999).

[71] M. Li, S. Yan, B. Yao, Y. Liang, G. Han, and P. Zhang, Optical trapping force and torque on spheroidal Rayleigh particles with arbitrary spatial orientations, J. Opt. Soc. Am. A **33**, 1341 (2016).

[72] O. Brzobohatý, V. Karásek, M. Šiler, L. Chvátal, T. Čižmár, and P. Zemánek, Experimental demonstration of optical transport, sorting and self-arrangement using a 'tractor beam', Nat. Photon. **7**, 123 (2013).

[73] R. Jáuregui and J. P. Torres, On the use of structured light in nonlinear optics studies of the symmetry group of a crystal, Sci. Rep. **6**, 20906 (2016).

[74] C. J. Sheppard, S. Rehman, N. K. Balla, E. Y. Yew, and T. W. Teng, Bessel beams: Effects of polarization, Opt. Commun. **282**, 4647 (2009).

[75] C. Bohren and D. Huffman, Absorption and scattering of light by small particles, in *Absorption and Scattering of Light by Small Particles* (John Wiley and Sons, Ltd., New York, 1998), Chap. 4, pp. 83–122.

[76] Absorption and scattering of light by small particles, in *Absorption and Scattering of Light by Small Particles* (John Wiley and Sons, Ltd., New York, 1998), Chap. 8, pp. 182–223.

[77] R. Ali, F. Pinheiro, R. Dutra, F. Rosa, and P. M. Neto, Probing the optical chiral response of single nanoparticles with optical tweezers, J. Opt. Soc. Am. B **37**, 2796 (2020).